Memoirs of the Faculty of Engineering, Okayama University, Vol.26, No. 2, pp.93-109, March 1992

Transport Simulasion in a Burning Tokamak Plasma

Atsushi FUKUYAMA*, Takashi KASAI* and Yoichiro FURUTANI*

(Received January 17 , 1992)

Synopsis

A one-dimensional tokamak transport code (TASK/TR) has been developed to analyze the evolution of a burning plasma accompanied with fusion reaction. This code deals with the electrons, deuterons, tritons, thermalized α particles, fast α particles and beam ions, separately, in order to describe the dependence of the reaction rate on the ion mixture ratio. As an energy transport model, the drift wave turbulence mode is employed. The heating and current drive by the neutral beam injection as well as the pellet injection for fuelling are also included. This code is applied to a reactor-grade plasma aimed at in the ITER project. The cases of an ignited plasma and a current-driven plasma are examined. The required power for full current drive is estimated. The effect of pellet injection, both fuel and impurity ions, is also studied.

1 INTRODUCTION

The nuclear fusion research by magnetic confinement has been extensively pursued by means of experiments on three large-scale tokamaks such as TFTR (USA), JET (EC) and JT-60 (JAPAN). For the present, a plasma of the highest performance is realized on JET tokamak with the major radius of 3 m, the minor radii of 1.25 m × 2.1 m and subject to the central magnetic-flux density of 3.45 T. This plasma is characterized by the central ion temperature of 10 keV, the central ion density of $0.7 \times 10^{20}\,\mathrm{m}^{-3}$ and the confinement time of 1.1 sec[1]. Though these data were obtained for a deuterium plasma, conversion into a plasma having the mixing ratio D : T = 1 : 1 yields the Q-factor of the order of 0.8, which implies that about 80 % of an injected heating power was converted into an output nuclear fusion power.

*Department of Electrical and Electronic Engineering

On the other hand, although a present-day discharge duration on large-scale tokamaks is less than 10 seconds, research aiming at a long-time operation is also in progress. On the JET tokamak, they realized a discharge longer than 20 seconds with a plasma current of 3 MA by means of the current drive using lower hybrid waves[2]. On the TRIAM-1M, the small-size superconducting tokamak of Kyushu University, they succeeded in the continuous operation exceeding one hour with the help of the current drive using also lower hybrid waves, despite their plasma properties of low density of $2 \times 10^{18}\,\mathrm{m}^{-3}$ and weak current of 25 kA[3].

Stimulated by such experimental evidences on tokamaks, specialists began to examine a next-generation tokamak device. The objective of the next apparatus is to attain a $Q = 5$ situation, in which heating by α-particles becomes of the same order as heating by external sources. The most concrete next device is the **I**nternational **T**hermonuclear **E**xperimental **R**eactor (ITER). In this ITER project, the four parties, EC, Japan, USA and USSR, collaborate on an equal footing under the auspices of the International Atomic Energy Agency (IAEA). The conceptual design put forth for three years since 1988 came to terms at the end of 1990 and a new agreement is settled to carry out a more detailed design for the next six-year period.

In a core plasma of the ITER, they aim at a long-time operation of several thousands seconds with $Q = 5$ and also at the attainment of $Q = 20$. If these objectives were realized, heating by α-particles of 3.5 MeV produced by fusion reaction in a core plasma would be dominant and these plasmas would be quite different in nature from the present-day heated plasmas. Furthermore, we do not know how and to what extent current drive by neutral beam injection and lower hybrid waves affect a plasma heated by α-particles. By this token, we need to understand a priori typical behaviours of a core plasma which does not exist yet in reality.

In this paper, we carry out a one-dimensional transport analysis of a nuclear burning plasma, visualizing a tokamak plasma of the ITER class and examine the effect of current drive and pellet injection. To this end, we have newly exploited a code for the one-dimensional transport analysis TASK/TR (abbreviation of **T**ransport **A**nalysis and **S**imulation for Tokama**K** / **TR**ansport).

With the help of this simulation codes, we shall analyze quantitatively a stationary distribution of a burning plasma and the plasma response to external disturbances. To our knowledge, transport phenomena in a tokamak plasma are not well elucidated yet and no reliable transport model capable of fully explaining experimental results is proposed. For this reason, we adopt in this work a model involving the drift-wave turbulence and neoclassical transports which are considered to be most compatible at the present time. As for the coefficients in the turbulent transport, we choose them such that a scaling law for energy confinement time inferred from the past experimental results be reproduced.

The paper is organized as follows. In the next chapter, we expound the one-dimensional transport equation for a tokamak plasma. We also explain the drift-wave turbulence transport model, the neutral beam absorption model, the pellet injection analysis model and so forth. Chapter 3 is devoted to plasma parameters used in the analysis and choice of transport coefficients. We show in Chapter 4 results of analysis on the stationary profile of the Joule-heated and current-driven plasmas, followed by the analysis of a plasma response to pellet injection. The last chapter is a

conclusion, in which we quote several topics to be settled in a near future.

2 BASIC EQUATIONS

2.1 Constituent Particles of Plasma

The constituent particles of a core plasma in the fusion reactor are : electron, deuteron and triton (fuel ions), α-particle produced by the nuclear fusion reactions and impurity ions. Since α-particles are produced by the nuclear reaction in a core plasma, ratios of the particle density vary with time. Produced α-particles of 3.5 MeV decelerate through Coulomb collisions and are thermalized. While high-energy α-particles decelerate via collision with electrons, thermalized α-particles mainly collide with fuel ions. By this token, we need to treat them as different species of particle. The confinement property of fast particles differs in nature from that of thermal particles. Inferred from the analysis of ion cyclotron wave heating, the confinement time of fast ions is considered to be longer than that of the deceleration time[5], so that we assume that they decelerate before whatever effect of the spatial diffusion takes place. As a result, we shall solve, for fast α-particles and beam ions, local evolution equations that do not contain any spatial transport. Moreover, since little is known about the transport of impurity ions, we assume that they do not change in time in the present analysis. We adopt the carbon (C) as a representative of low-Z impurities and iron (Fe) as that of high-Z impurity ions.

2.2 Transport Equations for Thermal Particles

Equations governing the particle and energy transport in a tokamak plasma are the equation of continuity and of energy conservation. We then are led to use the one-dimensional transport equation involving the plasma minor radius r as a sole variable, to analyze the radial transport. The two transport equations, coupled with Faraday's induction law, are given by[6,7]

$$\frac{\partial}{\partial t} n_s = -\frac{1}{r}\frac{\partial}{\partial r} r\Gamma_s + S_s, \tag{1}$$

$$\frac{\partial}{\partial t}\frac{3}{2} n_s T_s = -\frac{1}{r}\frac{\partial}{\partial r} r Q_s + P_s, \tag{2}$$

$$\frac{\partial}{\partial t} B_\theta = \frac{\partial}{\partial r} E_z, \tag{3}$$

where the suffix s denotes a physical quantity pertaining to the s-th species: e for electrons, D for deuterons, T for tritons and He for thermalized α particles. The quantities n_s, Γ_s, T_s and Q_s are the number density, the particle flux, the temperature and the heat flux, respectively. Also S_s and P_s stand, respectively, for the particle and energy source. B_θ is the poloidal magnetic field induced by plasma current and E_z the toroidal electric field. As for the electron density profile, we shall determine it such that the condition of electrical neutrality $n_e = \sum_i Z_i n_i$ holds, where Z_i is the ionic charge of the i-th species of ion.

We can also express Γ_s, Q_s and E_z as

$$\Gamma_s = v_s n_s - D_s \frac{\partial n_s}{\partial r}, \tag{4}$$

$$Q_s = v_s n_s T_s - n_s \chi_s \frac{\partial T_s}{\partial r} + \frac{3}{2} T_s \Gamma_s, \tag{5}$$

$$E_z = \eta J_{\rm OH} = \eta \left(\frac{1}{\mu_o} \frac{1}{r} \frac{\partial}{\partial r} r B_\theta - J_{\rm NB} - J_{\rm BS} \right), \tag{6}$$

Here v_s represents the radial velocity, D_s the diffusion coefficient of particle, χ_s the diffusion coefficient of heat, η the electrical resistivity, μ_0 the permeability in vacuo, $J_{\rm OH}$ the Joule (or ohmic) current, $J_{\rm NB}$ the driven current due to neutral beam injection (NBI) heating and $J_{\rm BS}$ the bootstrap current driven by density gradient. In eq.(6) we have made use of the Ampere's law.

The electrical resistivity is estimated by the use of the neoclassical theory which takes into consideration the inhomogeneity of the toroidal magnetic field. The particles source terms include the ionization of neutral atoms, the neutral beam injection, the the pellet injection and the production and loss of particles by nuclear fusion reaction. The energy source terms involves the energy partition coming from Coulomb collisions with other species of particles, the Joule heating, the heating due to the collision with beam ions and fast α-particles. The energy loss due to the charge exchange between neutral atoms and ions and the radiation loss owing to the line emission and the Bremsstrahlung is also included.

2.3 Evolution Equation for Fast Particles

As was described in §2-1, we assume that fast α-particles and fast beam ions do not contribute to the spatial transport and are decelerated on a magnetic surface on which they are created. Fast α-particles have the energy of 3.5 MeV, while fast beam ions are produced by injected energetic neutral beams and then decelerated through the Coulomb collision with electrons and ions. Therefore, the velocity distribution of the b-th particle can be approximated by the slowing down distribution

$$f(v) = \frac{S_{\rm b} \tau_{\rm sb}}{4\pi} \frac{1}{v^3 + v_{\rm c}^3} \Theta(v_{\rm b} - v), \tag{7}$$

where $S_{\rm b}$ is the creation rate of the b-th particle, $\tau_{\rm sb}$ the deceleration time due to the electron collision

$$\tau_{\rm sb} = \frac{6\pi\sqrt{2\pi}\varepsilon_0^2 m_{\rm b} T_{\rm e}^{3/2}}{n_{\rm e} Z_{\rm b}^2 m_{\rm e}^{1/2} e^4 \ln \Lambda}, \tag{8}$$

where e is the unit charge, m_s the mass of the s-th species, T_s the temperature of the species s, $\ln \Lambda$ the Coulomb logarithm and ε_0 the electrical susceptibility. The critical velocity at which the collision rate with the electron becomes of the same order as that with the ion is given by

$$v_{\rm c}^3 \equiv \sum_{\rm i} v_{\rm ci}^3 = \sum_{\rm i} 3\sqrt{\frac{\pi}{2}} \frac{n_{\rm i} Z_{\rm i}^2}{n_{\rm e}} \frac{m_{\rm e}}{m_{\rm i}} \left(\frac{T_{\rm e}}{m_{\rm e}} \right)^{3/2}. \tag{9}$$

Here $v_{\rm b}$ denotes a velocity just after the particle was created and $\Theta(x)$ is the Heaviside's step function.

When the velocity distribution takes the form, eq.(7), time evolution of the energy density $W_{\rm b}$ of the b-th particle is approximated by

$$\frac{\rm d}{{\rm d}t} W_{\rm b} = P_{\rm b} - \frac{W_{\rm b}}{\tau_{\rm b}}, \tag{10}$$

where P_b represents an input heating power and τ_b is so defined as to give a correct energy density at a stationary state, such that

$$\tau_b = \frac{1}{2}\tau_s \left[1 - H\left(\frac{v_b}{v_c}\right)\right], \qquad \text{where} \quad H(y) \equiv \frac{2}{y^2}\int_0^y \frac{x}{x^3+1}dx. \tag{11}$$

The total power W_b/τ_b distributed on electrons and ions can be given, respectively, by

$$P_{be} = \frac{W_b}{\tau_b}\left[1 - H\left(\frac{v_b}{v_c}\right)\right], \qquad P_{bi} = \frac{W_b}{\tau_b}\frac{v_{ci}^3}{v_c^3} H\left(\frac{v_b}{v_c}\right). \tag{12}$$

When $v_b \gg v_c$, $H(v_b/v_c)$ approaches 0 and almost all the energy is transferred to electrons. As the particle and energy densities in the stationary state are given, respectively, by

$$n_b^{st} = \frac{1}{3} S_b \tau_{sb} \ln\left(1 + \frac{v_b}{v_c}\right), \tag{13}$$

$$W_b^{st} = S_b \tau_s \frac{1}{2} m_b v_b^2 \frac{1}{2}\left[1 - H\left(\frac{v_b}{v_c}\right)\right], \tag{14}$$

the particle density n_b for a given W_b is estimated as $n_b = n_b^{st} W_b / W_b^{st}$.

2.4 Transport Coefficients

Various theories on energy transport coefficients have been proposed, but none of them can yet fully explain experimental results. Experimentally measured values of the electron diffusion coefficient is by almost two order of magnitude larger than those predicted by the neoclassical theory. As for the ion diffusion coefficient, it is only several times larger than the predicted value but shows a different dependence on parameters. To try to explain the above mentioned anomalous transport phenomenon, the drift wave turbulence model[8] was devised.

According to this model, a number of drift waves are excited in the presence of microscopic instabilities and the plasma is considered to be in a turbulence state. The diffusion coefficient is estimated by the mixing length theory[9]. If we denote by γ and $k_\perp$ the linear growth rate of the wave and the wave number in the perpendicular direction, we take for granted that the diffusion coefficient is proportional to $\gamma/k_\perp^2$. We have estimated the diffusion coefficient for various modes of the electrostatic drift waves: the collisionless trapped electron mode, the dissipative trapped electron mode, the collisionless circulating electron mode, the dissipative circulating electron mode and the ion-temperature gradient mode. The explicit forms of these coefficients are given by Dominguez and Waltz[8].

By virtue of the condition of electrical neutrality, we can not apply this diffusion coefficients to the particle diffusion but, instead, can estimate by its direct use the diffusion coefficient for heat transport. We have also included the neoclassical heat diffusivity[10] which may contribute to the ion thermal transport near the magnetic axis.

As for the particle transport coefficients, no reliable theories are available up to now. We are then obliged to use experimental results and assume that they are free from any parameter dependence. In other words, we suppose that the diffusion coefficient is uniform in space and adjust the inward pinch speed v_s so that the stationary density profile be reproduced.

When there exist a radial density and temperature gradient, the toroidal current is induced by the neoclassical effect. It is termed the "bootstrap current" and sustains itself independently of any applied electric field. Recent experiments on large tokamaks confirmed the existence of the bootstrap current. We have used a formula given by Hinton and Hazeltine[11] and, for simplicity, have neglected the contribution of the beam component here.

2.5 NBI Heating and Current Drive

Energetic neutral particles injected into plasma transfer energy to ions through charge exchange, ionization and multistep ionization. The cross-section for beam stopping σ_b is provided as a function of the particle energy, the electron and ion densities and ion charge[12]. Let l to be the distance along a beam. The number of neutrals $N(l)$ evolves according to the equation

$$\frac{dN(l)}{dl} = -n_e \sigma_b N(l). \tag{15}$$

As can be seen from this equation, we can evaluate the production rate of fast particles from a decrease per unit length of the number of neutrals and thus the heating power P_b of beam ions. The created fast beam ions rotate along the magnetic surface during the deceleration and consequently give rise to the ion current j_i. Light electrons tend to keep pace with ions and thus the total current turns out to be

$$j_t = j_i(1 - Z_b/Z_{eff}), \tag{16}$$

where the effective charge of plasma Z_{eff} is defined by $\sum_i Z_i^2 n_i/n_e$. The second term in the parenthesis represents the electron current j_e flowing in the direction opposite to the ion current.

When account is taken of the neoclassical effect, the electron current decreases due to the presence of trapped electrons. Including these effects, the current-driven efficiency by means of NBI can be approximated by

$$\frac{j}{P_b} = \frac{2eZ_b\tau_{sb}}{m_b v_c}\left[1 - \frac{Z_b}{Z_{eff}}\{1 - G(Z_{eff}, \epsilon)\}\right] J_0\left(\frac{v_b}{v_c}, y\right). \tag{17}$$

The correction terms G and J_0 have been estimated by the Fokker-Planck analysis and the explicit forms are given in [15].

2.6 Pellet Injection and Ablation Model

As a nuclear burn progresses to a certain degree, the problem of replenishment of such fuels of nuclear fusion reaction as deuterium and tritium arises. When a neutral gas is injected from a circumferential region, the loss by charge exchange increases there. For this reason, a new scheme is being examined of injecting into a plasma a pellet which contains a frozen mixture of deuterium and tritium. Experiments of the pellet injection are in progress on tokamak and production of dense plasmas is reported. Moreover, improvement of the confinement is ascertained for the density profile with a peak at the center. We expect that the pellet injection is efficient not only for fuel supply but can be a useful tool for the control of an output of nuclear fusion and the improvement of the confinement by controlling the density profile.

In a hot, dense, large-scale plasma, however, we need to increase the pellet radius and the injection speed in order for the pellet to penetrate into a plasma center. It is conjectured that a speed of at least 5 km/s is required to keep an efficient penetration length. To this end, the pellet radius will be of the order of 5 mm. With such a size, however, a single pellet could cause a considerable perturbation in a plasma and thus we are urged to estimate quantitatively to what extent the pellet injection affects a plasma in a burning state.

A model adopted in the present analysis is the neutral-cloud screening model (NCSM)[13] widely accepted now. The basic idea of this model is explained thus. When a heat flow due to fast particles impinges on a pellet, they are decelerated by virtue of a neutral cloud already formed around the pellet. This mechanism determines an ablation rate. We note, however, that only electrons and fast α-particles are considered as fast particles in this work and that ablation by beam ions is neglected.

According to the NCSM, we have employed the reduction rate of the pellet radius given by [14] and have calculated the particle source.

3 MODEL OF THE PLASMA

3.1 Plasma Parameters

In this work we adopt the parameters employed in the conceptual design of the ITER, which may characterize a core plasma in a thermonuclear fusion reactor. They are listed as follows.

Plasma major radius	R	6 m
Plasma minor radius	a	2 m
Ellipticity	κ	2
Toroidal magnetic field	B_t	4.85 T
Plasma current	I_p	22 MA

We set the beam energy E_b for the NBI heating equal to 1 MeV.

3.2 Initial and Boundary Conditions

As for the spatial profile of the density, the temperature and the plasma current, we wish to reproduce a relatively flat density distribution and a parabolic temperature distribution as are usually observed on a large-scale tokamak. They are described as

$$n_s(r) = n_s(0)\left\{1-(r/1.05a)^2\right\}^{1/2}, \tag{18}$$

$$T_s(r) = \{T_s(0)-T_s(a)\}\left\{1-(r/a)^2\right\}+T_s(a), \tag{19}$$

$$J_{OH}(r) = J_{OH}(0)\left\{1-(r/a)^2\right\}, \tag{20}$$

The mixing ratio between deuterium and tritium is set equal to 1 : 1. With regard to the impurity densities, we took into account the density dependence[15] inferred from experimental results. Their density profiles are assumed to be proportional to the local electron density $n_e(r)$. The density of Fe is set equal to the one-tenth of the value recorded in [15]. This choice is relevant to a situation

that, at the build-up of a plasma, radiation loss in the circumferential region remains smaller than Joule loss. The neutral density is set equal to zero in this work.

An initial B_θ profile is derived from $J_{\rm OH}(r)$ of eq.(20). Since a value of $J_{\rm OH}(0)$ is unknown a priori, we determine it such that $B_\theta(a) = \mu_0 I_{\rm p}/2\pi\kappa' a$ hold, where κ' denotes the circumferential ellipticity. As we keep $I_{\rm p}$ constant during the Joule heating, we fix $B_\theta(a)$. During the current drive we do not fix $I_{\rm p}$ and thus $B_\theta(a)$ is determined by the circuit equation

$$\frac{{\rm d}B_\theta(a)}{{\rm d}t} = \frac{\mu_0}{2\pi\kappa' a}\frac{{\rm d}I_{\rm p}}{{\rm d}t} = -\frac{\mu_0}{2\pi\kappa' a}\frac{1}{L_{\rm p}}V_{\rm p}(a) = -\mu_0\frac{R}{\kappa' a}\frac{1}{L_{\rm p}}E_z(a), \tag{21}$$

where $L_{\rm p}$ is the inductance of the torus plasma [$= \mu_0 R\ln(8R/a - 2)$] and $V_{\rm p}$ the toroidal loop voltage.

On the other hand, the boundary conditions on the density and temperature are kept fixed, assuming that the initial conditions evaluated at $r = a$ remain unchanged.

3.3 Characteristics of the Transport Model

In the mixing length theory, there is an ambiguity of the transport coefficient of order unity. We have adjusted the coefficient so as to reproduce the experimental observations. Experimental results of the confinement properties in tokamaks are summarized in the form of an empirical scaling of the confinement time, $\tau_{\rm E}$, which is defined by the total energy stored in plasma divided by the heating power. In recent tokamak experiments, various kinds of operation modes, inclusive of the H-mode inclusive, are realized where the particle and energy confinement is improved. Since a lot of reliable experimental data have been accumulated on the usual operation mode (L-mode), however, we employ the most recent L-mode scaling[16] as a base line. This scaling is described as

$$\tau_{\rm E}^{\rm ITER89} = 0.048 M^{0.5} I_{\rm p}^{0.85} R^{1.2} a^{0.3} \kappa^{0.5} n^{0.1} B^{0.2} P^{-0.5}\,[\rm sec], \tag{22}$$

where M is the ion mass number, $I_{\rm p}$ the plasma current in MA, R the major radius in m, a the minor radius in m, κ the ellipticity, n the line average density in unit of $10^{20}\,{\rm m}^{-3}$, B the toroidal magnetic field in T and P the heating power in MW.

We have chosen the number coefficient such that $\tau_{\rm E}$ of a deuterium plasma becomes 1.5 times larger than that as obtained from eq.(22) in a Joule heating phase. This enhancement factor is rather modest compared with the average improvement factor of about 2 in the H-mode.

We have examined various parameter dependence of $\tau_{\rm E}$ and compare the dependence of $\tau_{\rm E}^{\rm ITER89}$ scaling law. For the input power, the results of our simulation model are in good agreement with $\tau_{\rm E}^{\rm ITER89}$ law. Dependence on the average density agrees fairly well with $\tau_{\rm E}^{\rm ITER89}$ prediction for high density, though at low density an agreement is poor. In the course of the NBI heating, the density dependence is weak as in the scaling law. For the toroidal magnetic field and the plasma current, however, $\tau_{\rm E}$ is approximately proportional to $B_{\rm T}$ and independent of $I_{\rm P}$. This difference from the scaling law indicates a limit of applicability of the drift-wave turbulence model. In the analysis below, however, there arises no difficulty if we work with almost fixed $I_{\rm p}$ and $B_{\rm t}$.

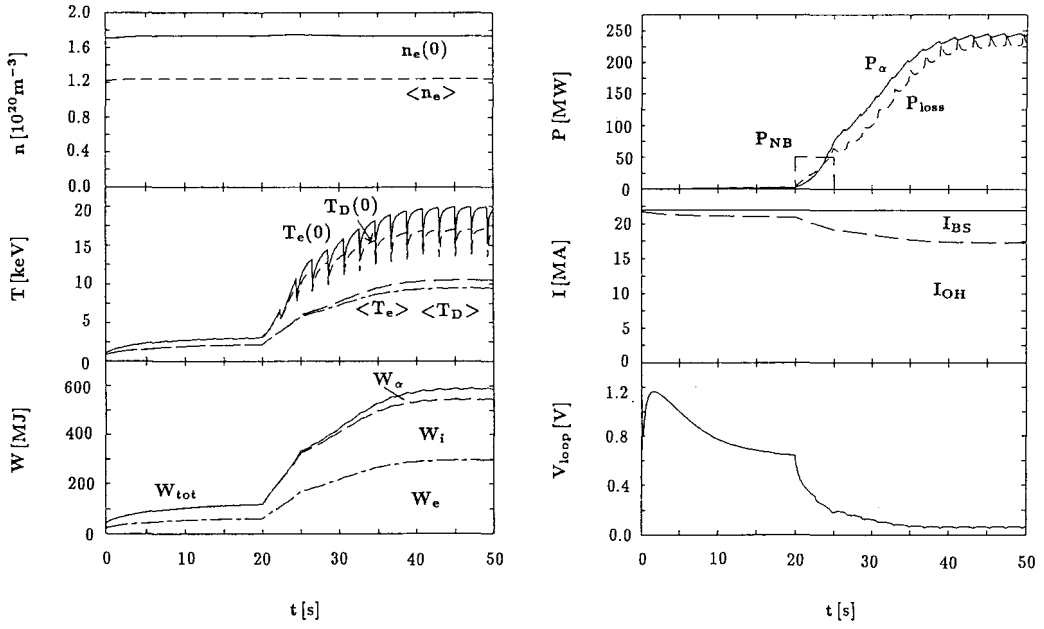

Figure 1: Temporal evolution of the plasma parameters in the case of the ignited plasma.

4 RESULTS OF NUMERICAL ANALYSIS

4.1 Ignition of a Burning Plasma

Since a fusion output power is proportional to the square of a plasma density, Q rises with increasing plasma density. In the case of low density plasma, additional heating is necessary to sustain the burning plasma. When the plasma density exceeds a certain critical value $n_{\rm crit}$, however, α-particle heating itself becomes sufficient to keep the burning state. This transition to the burning state without external heating is called ignition.

In order to achieve the ignition, the plasma has to be heated to several keV. Figure 1 shows an example of the simulation result on the ignition. The figure shows the temporal evolution of the density, the temperature, the stored energy, the heating and loss power, the plasma current and the toroidal loop voltage. The quantities with <> represent the volume-averaged value. After the Joule heating, the NBI heating of 50 MW is applied for 5 sec. The central ion temperature begins to increase until the steady state of 17 kev is obtained. The oscillation of the temperature is due to the effect of sawtooth oscillation introduced to simulate the experimental observation. In this case, the fusion output power, 5 times the α-particle heating power P_α, exceeds 1 GW.

The loop voltage in the ignited state is 0.06 V. According to the conceptual design of ITER, the poloidal magnetic flux available in a burning state is about 100 V sec. Therefore the burning time of 1600 sec is expected from the present analysis.

It should be noted that the critical density $n_{\rm crit}$ for ignition depends on the transport model used. We found that $n_{\rm crit}$ increases almost linearly with the increase of transport coefficient.

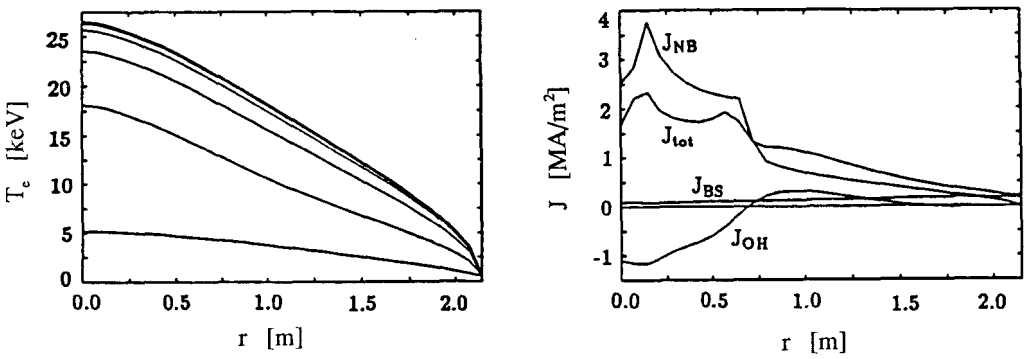

Figure 2: Radial profiles of the electron temperature and the plasma current density.

4.2 Current-Driven Plasma

In order to sustain a long burning state, it is necessary to drive the plasma current externally. Since the current drive efficiency is inversely proportional to the plasma density, a low-density operation with less fusion output is required for efficient current drive.

We show the results in the case of the current drive by NBI. In Fig. 2, we illustrate both the temperature and current profiles after a plasma attains a stationary state by NBI. This is the case for $<n_e> \sim 0.7 \times 10^{20}\,\mathrm{m}^{-3}$ and NBI input power of 150 MW. We observe a peak of the absorbed power near the axis $r = 0.35\,\mathrm{m}$ corresponding to the tangential radius of the NBI beam and, at its vicinity, a peak of the NBI driven current also. The bootstrap current flows in the circumferential region where a pressure gradient is large. When a current is driven by NBI, a counter electric field is induced there and a counter Joule current flows. In order for the spatial profile of the total current to vary, a variation of the poloidal magnetic flux is required, but the latter varies slowly due to a low resistivity of a hot plasma. The diffusion coefficient of the magnetic flux η/μ_0 becomes $10^{-3}\,\mathrm{m}^2/\mathrm{s}$ for $T_e = 10\,\mathrm{keV}$. For this reason, several hundreds of seconds should elapse for a variation of the total current profile and during this interval a counter electric field is maintained.

Figure 3 indicates the density dependence of the current at high input power ($P_{\mathrm{NB}} = 150\,\mathrm{MW}$). With increasing densities, the collision between the beam and the plasma becomes frequent, the current drive efficiency lowers and the driven current decreases. For high densities the pressure gradient steepens and the bootstrap current increases. In the low density region, the current drive efficiency is high, Joule current flows in the counter direction and the primary coil side is recharged. With increasing densities, the counter Joule current decreases but, sooner, an increase of the bootstrap current overshoots a reduction of the driven current and the counter Joule current begins to increase again.

Finally, we examined the power dependence of the current for a fixed density. The driven current increases with the input power in both the high density ($1.2 \times 10^{20}\,\mathrm{m}^{-3}$) and low density ($0.7 \times 10^{20}\,\mathrm{m}^{-3}$) cases as shown in Fig. 4. In the low density case, the electron temperature rises with increasing input power, the current drive efficiency is improved and thus electron temperature rises faster than linearly. With increasing input power, the bootstrap current increases rapidly

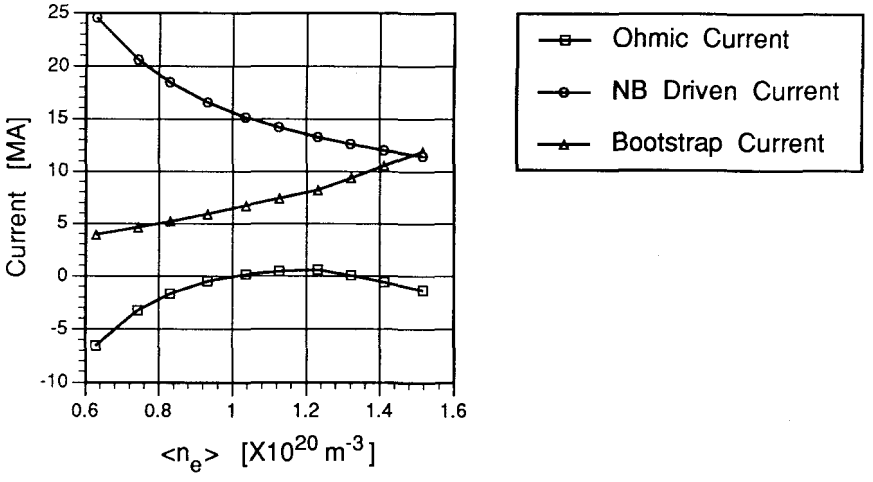

Figure 3: Density dependence of the plasma current

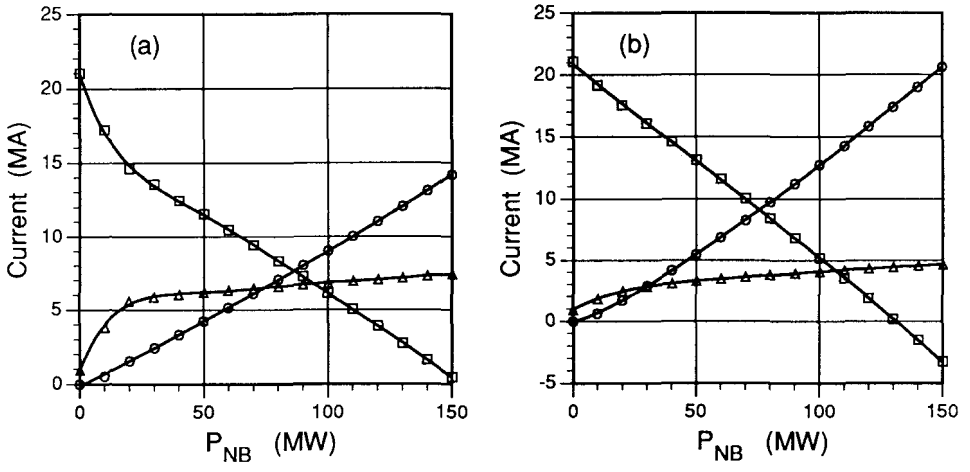

Figure 4: Plasma current as a function of the NBI power. (a) the high density case and (b) the low density case. Symbols are the same as those in Fig. 3

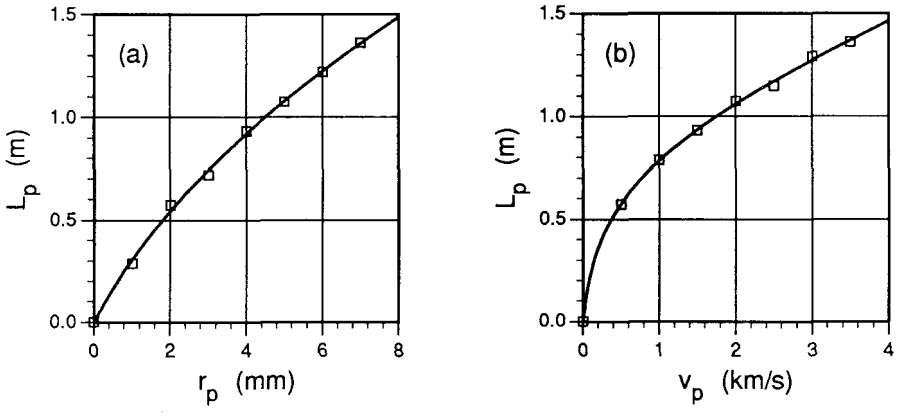

Figure 5: Dependence of the penetration length l_p on the pellet radius r_p and the injection speed v_p.

with the increase of the temperature and, after it attains a certain value, increases gently. From this Fig. 4, we see that the bootstrap current is large for the high density, but that the current drive efficiency decreases. In the case of the low density, the Joule current completely disappears at $P_{NB} = 130\,\mathrm{MW}$ but in the case of a high density, we require 150 MW.

4.3 Effect of the Pellet Injection

Before calculating an output variation by the pellet injection (abbreviated as PI below), we wish to examine a relationship among a pellet radius, an injection speed and a penetration length. To this end, we injected a pellet into the stationary current-driven plasma with the average electron density $<n_e> \sim 0.7 \times 10^{20}\,\mathrm{m}^{-3}$ by means of NBI heating of 130 MW, by varying its radius and injection speed. Figure 5(a) shows the penetration length L_p versus r_p, with v_p fixed to 2 km/sec, indicating that L_p increases with r_p as $r_p^{0.8}$. On the contrary, we observe in Fig. 5(b) that, with r_p fixed to 5 mm, L_p increases with v_p as $v_p^{0.4}$. In the subsequent analysis, we varied a magnitude of the density variation by adjusting the injection speed to keep the penetration length to be $L_p \sim a/2 = 1.075\,\mathrm{m}$ and by varying the pellet radius.

4.3.1 Case of injecting the fuel pellet injection into a Joule plasma

When we injected a fuel pellet into a self burning plasma, the nuclear fusion output once decreases, but it immediately increases again due to the injection effect of the fuel pellet. By virtue of an increase of the nuclear fusion output, the input power grows up, so that the temperature which fell rapidly just after the PI rises higher than that before the PI.

We examined how a variation of the fusion output depend on a density variation resulting from the PI. The results are depicted in Fig. 6. It shows that the increment of the fusion output is nearly proportional to the density variation.

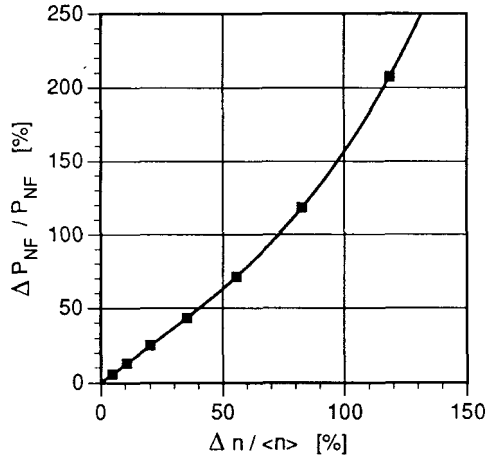

Figure 6: Increment of the fusion output power versus variation of the average density.

4.3.2 Case of injecting the impurity (He) pellet into a Joule plasma

In an ignited plasma, it is difficult to immediately reduce the fusion output by controlling the external heating power or the transport characteristics. The impurity injection is one of the promising schemes to shut down the plasma immediately in case of emergency. As indicated in Fig. 7, injection of the He pellet into a self burning plasma, as an example of the impurity pellet, is accompanied by an abrupt decrease of the output power, in contrast to the case of the fuel pellet.

In the typical case of Fig. 7, $\Delta P_{\rm NF}/P_{\rm NF} \sim 0.40$ was attained for $\Delta n/<n> \sim 0.40$ and $\Delta P_{\rm NF}/P_{\rm NF} \sim 1.00$ for $\Delta n/<n> \sim 4.00$. At this stage, the fusion reaction stops but, goes back to a state before pellet injection after several tens of seconds.

4.3.3 Case of injecting the fuel pellet into a current-driven plasma

When we inject a fuel pellet into a plasma which is current-driven by NBI, the drive efficiency lowers due to an increase of the plasma density. We study the dynamic response of the steady-state operation mode (almost full current-drive by 140 MW NBI) against the pellet injection. Figure 8 illustrate a typical example of simulation result. In consequence of the injection, rapid reduction and slow increase of th temperature occur. There appear transient peaks of the stored energy $W_{\rm tot}$, the fusion output P_α and the thermal loss to the plasma surface $P_{\rm loss}$. The pulsive reduction of the beam driven current $I_{\rm NB}$ is compensated by the increment of the inductive current $I_{\rm OH}$, since the total current changes very slowly in the L/R time scale. Peak in $P_{\rm loss}$ causes the increased pressure gradient in the edge region and the bootstrap current $I_{\rm BS}$ increases with a slower time scale. After 10 seconds, the plasma comes back to the original parameter. The variation of the fusion output for the typical example as shown in Fig. 8 yields $\Delta P_{\rm NF}/P_{\rm NF} \sim 1.0$ and $\Delta P_{\rm loss}/P_{\rm loss} \sim 0.3$ for $\Delta n/<n> \sim 1.0$.

The time evolution of the density and the temperature profiles is shown in Fig. 9. The temperature reduction propagates to the axis more rapidly than the density perturbation which

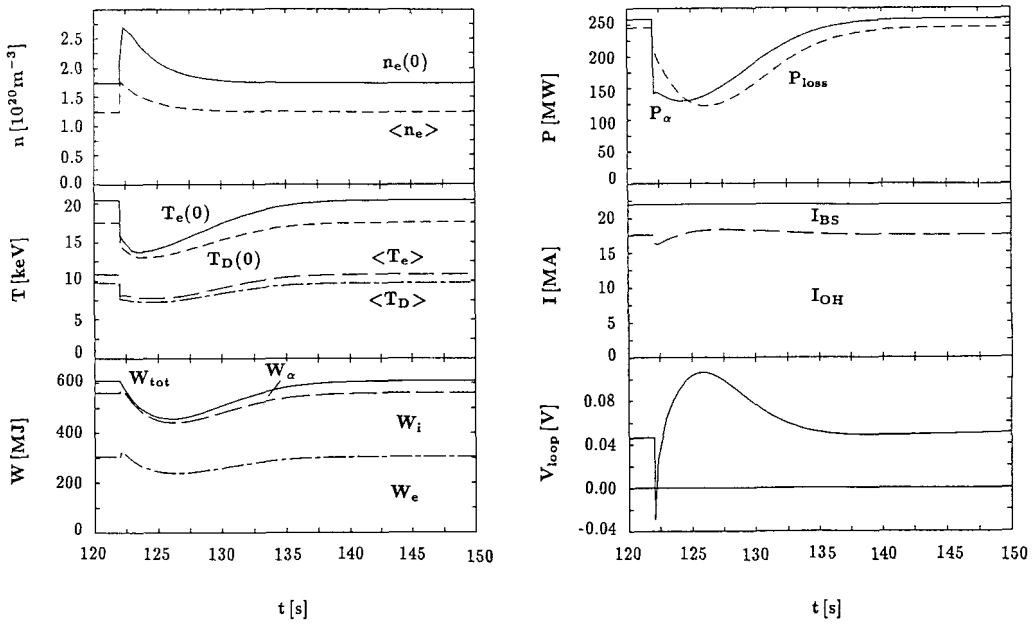

Figure 7: Temporal evolution of the plasma parameters in the case of the He pellet injection.

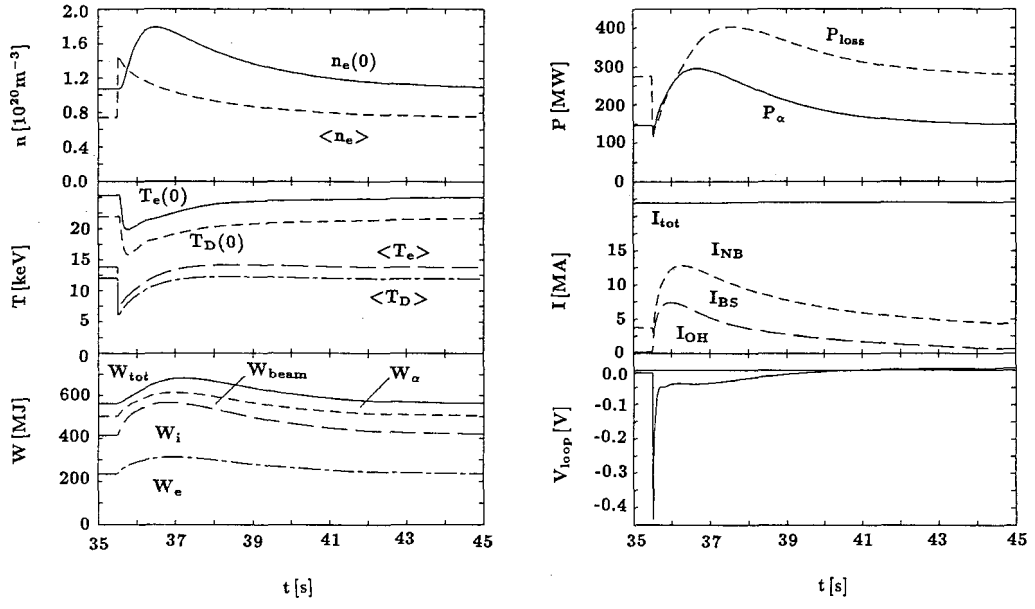

Figure 8: Temporal evolution of the plasma parameters in the case of the fuel pellet injection to the current-driven plasma.

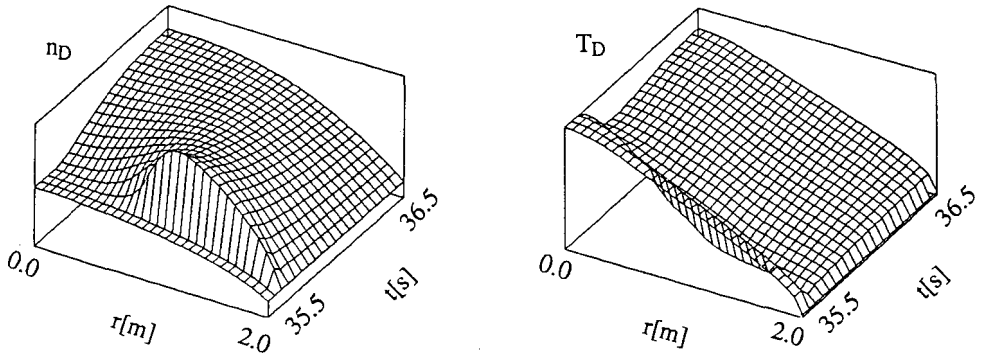

Figure 9: Temporal evolution of the ion density n_D and the ion temperature T_D profiles.

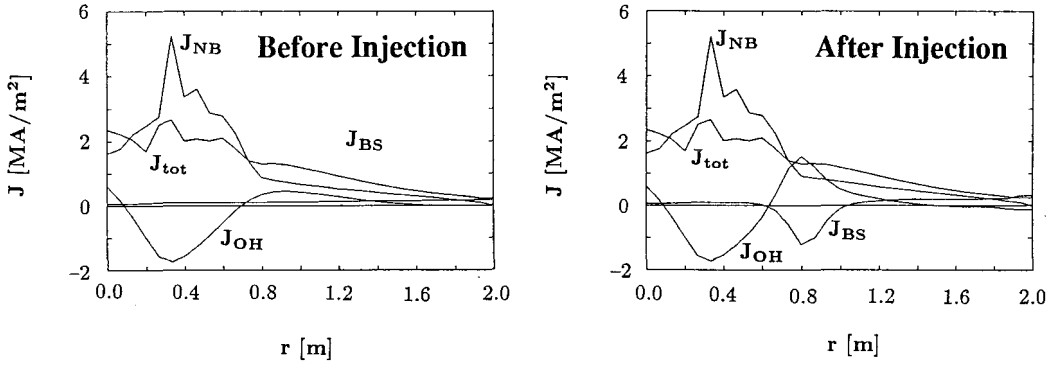

Figure 10: Current profiles just before and after the pellet injection

takes about 1 seconds. The current profile just before and after the pellet injection is depicted in Fig. 10. Since the density gradient is reversed by the injection, the bootstrap current becomes negative there.

5 CONCLUSION

To analyze the temporal evolution of a core plasma in a nuclear fusion reactor of the magnetic confinement type, we have exploited the code for the one-dimensional transport analysis TASK/TR and have applied it to the analysis of a tokamak plasma of ITER class. We thereby obtained a stationary profile of all the physical quantities of interest for various parameters and examined the dynamic response to an external disturbance.

In the analysis of the high-density case, we showed that the additional heating of a short period is enough to achieve the burning state. We elucidated that this n_{crit} is proportional to the heat diffusion coefficient χ. In the analysis of a current-driven plasma by NBI, we ascertained that the driven current is nearly proportional to the input power and also showed that, with increasing

densities, the current-drive efficiency lowers but the bootstrap current increases. Thus it may be feasible to maintain a perfect current drive with no Joule current flowing.

In the next step, we analyzed the effects on a plasma of the density variation caused by the pellet injection, in view of the fuel replenishment and the control of density profile and so forth. In both cases of the Joule plasma and the current-driven plasma, the temperature lowers and the output power of nuclear fusion P_{NF} once decreases as a result of the pellet injection but, with increasing temperatures, P_{NF} increases and exceeds a value it took before the pellet injection. We clarified that the loss power due to heat conduction P_{loss} which represents a heat flux into the divertor takes on a maximum value with a delay of the order of the energy confinement time relative to P_{NF}. When the density variation due to the pellet injection becomes $\Delta n \sim <n>$, *viz.*, the density doubles, both P_{NF} and P_{loss} double, compared with their values before the pellet injection. We also analyzed the case of injection of the impurity pellet to lower the output and found that, by doubling the density, P_{NF} and P_{loss} could be halved.

In this study, we elucidated the properties of the plasma response to various external disturbances and established a new scheme of use in quantitative analysis. Nevertheless there still remain certain ambiguities in our results, because we were obliged to adopt semi-empirical formulae for the heat and particle transport. It seems therefore indispensable to gain further understanding of the transport mechanisms in a tokamak plasma in the task of improving an accuracy of prediction for a nuclear burning plasma.

Acknowledgements

The authors appreciate valuable discussions with Dr. K. Itoh and Dr. S.-I. Itoh of the National Institute for Fusion Science.

References

[1] The JET Team: Proc. of 13th Int. Conf. on Plasma Physics and Controlled Nuclear Fusion Research (Washington, DC, 1990) Vol. 1, p. 27.

[2] C. Gormezano: Proc. of Tripartite Workshop on Current Drive and Plasma Stabilization (Naka, 1990).

[3] S. Itoh, N. Hiraki, Y. Nakamura *et al.*: Proc. of 13th Int. Conf. on Plasma Physics and Controlled Nuclear Fusion Research (Washington, DC, 1990) Vol. 1, p. 733.

[4] S.-I. Itoh, A. Fukuyama, T. Takizuka and K. Itoh: Fusion Technology **16** (1989) 346.

[5] T. Fujii, H. Kimura, M. Saigusa *et al.*: Proc. of 12th Int. Conf. on Plasma Physics and Controlled Nuclear Fusion Research (Nice, 1988) Vol. 1, p. 605.

[6] D. F. Düchs, D. E. Post and P. H. Rutherford: Nucl. Fusion **17** (1977) 565.

[7] T. Morishita, A. Fukuyama and Y. Furutani: J. Phys. Soc. Jpn., **57** (1988) 1238.

[8] R. R. Dominguez and R. E. Waltz : Nuclear Fusion **27** (1987) 65.

[9] B. B. Kadomtsev: *Plasma Turbulence* (Academic Press, New York, 1965).

[10] C. S. Chang and F. L. Hinton : Phys. Fluids **25** (1982) 1493.

[11] F. L. Hinton and R. D. Hazeltine : Rev. Mod. Phys. **48** (1970) 239.

[12] R. K. Janev, C. D. Boley and D. E. Post: Nuclear Fusion **29** (1989) 2125.

[13] P. B. Parks and R. J. Turnbull : Phys. Fluids **21** (1978) 1735.

[14] S. K. Ho and L. John Perkins : Fusion Technology **14** (1989) 1314.

[15] N. A. Uckan and ITER Physics Group : ITER Physic Design Guidelines : 1989, ITER Documentation Series, No.10 (1990).

[16] P. N. Yushmanov, T. Takizuka, K. S. Reidel *et al.* : Nuclear Fusion **30** (1990) 1999.